Charged Residues at the First Transmembrane Region Contribute to the Voltage Dependence of the Slow Gate of Connexins*

Bernardo I. Pinto[‡], Isaac E. García[‡], Amaury Pupo[‡], Mauricio A. Retamal[§], Agustín D. Martínez[‡], Ramón Latorre[‡1], and Carlos González[‡2]

From the [‡]Centro Interdisciplinario de Neurociencias de Valparaíso, Universidad de Valparaíso, Valparaíso 2360102 and the [§]Centro de Fisiología Celular e Integrativa, Facultad de Medicina, Clínica Alemana Universidad del Desarrollo, Santiago 7710162, Chile

Connexins (Cxs) are a family of membrane-spanning proteins that form gap junction channels and hemichannels. Connexin-based channels exhibit two distinct voltage-dependent gating mechanisms termed slow and fast gating. Residues located at the C terminus of the first transmembrane segment (TM-1) are important structural components of the slow gate. Here, we determined the role of the charged residues at the end of TM-1 in voltage sensing in Cx26, Cx46, and Cx50. Conductance/voltage curves obtained from tail currents together with kinetics analysis reveal that the fast and slow gates of Cx26 involves the movement of two and four charges across the electric field, respectively. Primary sequence alignment of different Cxs shows the presence of well conserved glutamate residues in the C terminus of TM-1; only Cx26 contains a lysine in that position (lysine 41). Neutralization of lysine 41 in Cx26 increases the voltage dependence of the slow gate. Swapping of lysine 41 with glutamate 42 maintains the voltage dependence. In Cx46, neutralization of negative charges or addition of a positive charge in the Cx26 equivalent region reduced the slow gate voltage dependence. In Cx50, the addition of a glutamate in the same region decreased the voltage dependence, and the neutralization of a negative charge increased it. These results indicate that the charges at the end of TM-1 are part of the slow gate voltage sensor in Cxs. The fact that Cx42, which has no charge in this region, still presents voltage-dependent slow gating suggests that charges still unidentified also contribute to the slow gate voltage sensitivity.

Cxs[3] are a family of membrane-spanning proteins involved in intercellular and paracrine/autocrine cellular communication. There are 21 human Cx genes that are widely expressed in virtually all human tissues (1). The topology of Cxs involves four transmembrane (TM) segments connected through two extracellular loops (EL) and one intracellular loop, and the N and C termini are facing the cytoplasm (2, 3). Cx monomers oligomerize in hexamers, which traffic to the plasma membrane and form connexons or hemichannels that can act as plasma membrane channels or can travel to intercellular contact zones, where they form intercellular channels known as gap junctions (GJs) (4). Cx-based channels can be regulated by different mechanisms such as redox signaling (5), metabolic inhibition (6), phosphorylation (7), and membrane voltage (8–10).

Although the voltage sensor domain of Cxs has not been clearly established, there is evidence suggesting that residues lining the pore of the channel are involved in transjunctional voltage dependence in GJs (11). In Cx-based channels, two voltage-dependent gating mechanisms can be distinguished, slow or loop gating and fast or Vj gating (12). The term fast gating is used to describe the transition of the channel between the open and subconductance state, supposedly related to an occlusion of the conduction pathway by the N terminus (3, 13). In contrast, in slow gating the channel transits through several intermediate conductances between the open and the fully closed states (14). This has been related to a turn of the 3_{10}-helix region at the end of TM-1 (3, 15). The GJ voltage dependence varies in its magnitude and polarity among different Cxs (12). For example, Cx26 GJ closes at positive potentials, and Cx32 closes at negative potentials. In heterotypic GJs formed by Cx26 and Cx32, the channel closes only when the Cx26 side is positive (16). The amino acids located in the N terminus of the protein define these differences in polarity. In regard to Cx26 and Cx32, the identity of the second amino acid in the N terminus defines the polarity of closing. If the second amino acid is neutral or positively charged, closing occurs at negative potentials. Otherwise, if it is negatively charged, positive potentials close the channel (10). Insertion of negatively charged residues up to the 10th position of the N terminus of Cx32 can reverse the polarity of the fast gate, suggesting that in this region of the

TABLE 1
Site-directed mutagenesis primers

Mutant	Primer	Sequence
Cx26_K41N	hCx26_K41N_fw	cctcgttgtggctgcaaatgaggtgtggg
	hCx26_K41N_rv	cccacacctcatttgcagccacaacgagg
Cx26_E42Q	hCx26_E42Q_fw	catctccccacacctgctttgcagccacaac
	hCx26_E42Q_rv	gttgtggctgcaaagcaggtgtggggagatg
Cx26_K41N_E42Q	hCx26_K41N_E42Q_fw	cctcgttgtggctgcaaatcaggtgtggg
	hCx26_K41N_E42Q_rv	cccacacctgatttgcagccacaacgagg
Cx26_K41E	hCx26_K41E_fw	ctcgttgtggctgcagaggaggtgtggg
	hCx26_K41E_rv	cccacacctcctctgcagccacaacgag
Cx26_K41E_E42K	hCx26_K41E_E42K_fw	gttgtggctgcagagaaggtgtggggagatg
	hCx26_K41E_E42K_rv	catctccccacaccttctctgcagccacaac
Cx46_E42Q	rCx46_E42Q_Fw	gggcggcagcccaggaggtgtgg
	rCx46_E42Q_Rv	ccacacctcctgggctgccgccc
Cx46_E43Q	rCx46_E43Q_Fw	cggcagccgagcaggtgtggggtg
	rCx46_E43Q_Rv	cacccacacctgctcggctgccg
Cx46_E42Q_E43Q	rCx46_E42Q_E43Q_fw	gggcggcagcccagcaggtgtgg
	rCx46_E42Q_E43Q_rv	ccacacctgctgggctgccgccc
Cx46_E42K	rCx46_E42K_fw	gggcggcagccaaggaggtgtgg
	rCx46_E42K_rv	ccacacctccttggctgccgccc
Cx46_E43K	rCx46_E43K_Fw	gcggcagccgagaaggtgtggggtg
	rCx46_E43K_Rv	cacccacaccttctcggctgccgc
Cx50_E42Q	mCx50_E42Q_Fw	cgggacagcagcgcagtttgtgtgggg
	mCx50_E42Q_Rv	ccccacacaaactgcgctgctgtcccg
Cx50_F43E	mCx50_F43E_Fw	gggacagcagcggaggaggtgtggggcgatgag
	mCx50_F43E_Rv	ctcatcgccccacacctcctccgctgctgtccc

N terminus there is a voltage drop that can be "sensed" by charged residues (17).

The structure of Cx26 channel supports the previously proposed model, which showed that the N terminus is located inside the pore of the channel. Because of charged residues in this segment, the N terminus acts as a fast gate particle in a voltage-dependent way (3, 13). Charged residues at the end of TM-1 also seem to play a role in the voltage dependence of Cx26 and Cx32 GJs (10, 18).

Because hemichannels have been studied in less detail than GJs, measurements of their voltage dependence are scarce. To determine the voltage dependence of Cx hemichannels, it could be useful to consider that in some Cxs both gates have different polarities, so they can be studied separately. Cx26, Cx46, and Cx50 are good candidates, because their conductance/voltage (*G/V*) relationship gives a bell-shaped curve (19 –21).

The slow gating mechanism in Cx26 hemichannels has been associated with a conformational change of the TM-1/EL-1 region of the protein. This change is most likely a rotation of the helix, which would close the channel (22). Mutations in this region are known to affect the voltage dependence of GJCs, but their particular effects on slow gating are unknown (10, 18).

This study was undertaken with the purpose of defining the molecular determinants of voltage-dependent slow gating in Cx26, Cx46, and Cx50 hemichannels. In Cx26, neutralization of lysine 41 decreases the voltage dependence of the fast gate and increases that of the slow gate, and swapping lysine 41 and glutamate 42 does not change the voltage dependence of the slow gating mechanism but increases that of the fast gating mechanism. We further studied the voltage modulation mechanism by TM-1 charges in slow gating of Cx50 and Cx46, where there are one and two negatively charged glutamate residues, respectively. In Cx46, glutamate neutralization decreased the voltage dependence of the slow gate, and glutamate mutation to lysine further decreased this voltage dependence. In contrast, in Cx50 the neutralization of the glutamate residue in this region increased the voltage dependence of the slow gating, and the

addition of a new glutamate residue decreased the voltage dependence. Cx42, which not contain any charged residues in this region, still presents voltage-gated slow gating. It is concluded that charged residues at the end of TM-1 are part of the voltage sensor of the slow gate of Cx hemichannels.

Experimental Procedures

Sequence Alignment—Cx sequences were identified by performing a Delta Blast (23) against the Swiss-Prot database (24) for human Cx23, Cx26, and Cx36, chicken Cx45, and rat Cx46 iteratively until no new sequences appeared. All resulting sequences were combined, and redundant sequences were eliminated to a total of 481 non-redundant sequences. These sequences were aligned using MAFFT (25), with the LINSI protocol.

Generation of Mutants and in Vitro Transcription—Human Cx26 pGEM was kindly provided by Dr. Jorge Contreras. Rat Cx46 pSP64 and mouse Cx50 pSP64 were kindly provided by Dr. Lisa Ebihara. Chicken Cx42 pBluescript KS+ was kindly provided by Dr. Viviana Berthoud. Mutations were introduced using the QuikChange site-directed mutagenesis kit (Stratagene). The primers used to generate the mutants are shown in Table 1. The coding region of the mutant was sequenced (Macrogen, Seoul, Korea) to confirm the mutation. Cx26 DNA was linearized by using the NheI enzyme (New England Biolabs); Cx46 and Cx50 DNAs were linearized with the EcoRI enzyme (Fermentas); Cx42 DNA was linearized with NotI enzyme (New England Biolabs). The linearized DNAs were transcribed with the *in vitro* transcription kit T7 mMessagemMachine or SP6 mMessagemMachine systems (Ambion) following the manufacturer's instructions.

Expression in Xenopus laevis Oocytes—*X. laevis* ovaries were obtained through ovariectomy. The oocytes were treated with collagenase IV A (Worthington). Stage V and VI oocytes were selected, defolliculated, and injected with 50 – 0.5 ng of the RNA, plus Cx38 antisense, to null endogenous expression of Cx38 (26). Oocytes were incubated at 17 °C in ND96 medium

containing (in mM) 96 NaCl, 1 KCl, 1 MgCl$_2$, 10 HEPES, and 1.8 CaCl$_2$. Hemichannel currents were recorded 24–72 h after injection.

Electrophysiology—Hemichannel currents were recorded using the two-electrode voltage clamp technique with an "oocyte clamp" amplifier (Warner Instruments). Electrodes were filled with a 3 M KCl solution and exhibited resistances between 0.5 and 2 megaohms. The bath solution contained (in mM) 88 choline chloride, 1 KCl, 1 MgCl$_2$, and 10 HEPES adjusted to pH 7.4. Macroscopic currents were acquired at 1 kHz using an analog to digital converter "Digidata 1200" (Axon Instruments).

Data Analysis and Equations—The $I_i(V)/I_{max}$ relation was obtained for Cx26, Cx42, Cx46, and Cx50 from the steady state of the macroscopic tail currents. In the case of Cx26, this curve was fitted with the three-state kinetic model. For this model, the equilibrium constants for the slow (K_s) and fast (K_f) gates were defined as shown in Equations 1 and 2,

$$K_s = \frac{O_1}{C} = e^{\frac{z_sF(V - V_s)}{RT}} \tag{Eq. 1}$$

$$K_f = \frac{O_2}{O_1} = e^{\frac{z_fF(V - V_f)}{RT}} \tag{Eq. 2}$$

where z_s and z_f are the equivalent gating charges ($z\delta$, or the number of charges z multiplied by a fraction of the field δ they cross) of the slow and fast gates, respectively; V is the membrane voltage; V_s and V_f are the voltages at which K_s and K_f are equal to 1, respectively; and R, T, and F have their usual meanings.

By using these equations we can write the relative probability of the state O_1 (P_{O1}) and O_2 (P_{O2}) as shown in Equations 3 and 4,

$$P_{O1} = \frac{K_s}{1 + K_s + K_s \cdot K_f} \tag{Eq. 3}$$

$$P_{O2} = \frac{K_s \cdot K_f}{1 + K_s + K_s \cdot K_f} \tag{Eq. 4}$$

The current I in the steady state will be given by the relative probabilities of the open states shown in Equation 5,

$$I(V) = (V - V_{rev}) \times (g_{O1}P_{O1} + g_{O2}P_{O2}) \tag{Eq. 5}$$

where V_{rev} is the reversal potential; and g_{O1} and g_{O2} are the conductance of the O_1 and O_2 states. If the tail currents I_i are used and data are normalized for the maximal tail current I_{max}, the $I_i(V)/I_{max}$ relationship would be as shown in Equation 6,

$$\frac{I_i(V)}{I_{max}} = \frac{P_{O1} + \dfrac{p_{O2} \cdot g_{O2}}{g_{O1}}}{P_{O1M} + \dfrac{P_{O2M} \cdot g_{O2}}{g_{O1}}} \tag{Eq. 6}$$

where I_i is the tail current of the ith trace; I_{max} is the maximum tail current, and P_{O1M} and P_{O2M} are the probabilities of the O_1 and O_2 states at I_{max}. For human Cx26, it has been observed that the relationship between the conductance of the subconductance state and the open state is about 0.11 (21).

TABLE 2
Apparent gating charges of the rate constants that describe the fast gate of WT Cx26 and mutants

	WT Cx26	Cx26_K41N	Cx26_K41E_E42K
$z_\alpha (e_0)$	2.0 ± 0.2	1.6 ± 0.1	1.9 ± 0.2
$z_\beta (e_0)$	1.9 ± 0.2	0.7 ± 0.2[a]	2.6 ± 0.2[a]
V_f	62 ± 2	38 ± 2[a]	50 ± 2[a]

[a] $p < 0.01$ using F test. Data were calculated using linearized Equations 10 and 11.

Because the slow gate can be easily separated from the fast gate for Cx42, Cx46, and Cx50, the $I_i(V)/I_{max}$ data were fitted using two-state model. In this case the tail current data (I_i) is well fitted using the Boltzmann equation (Equation 7),

$$I_i(V) = \frac{I_{max}}{1 + e^{\frac{z_sF(V - V_s)}{RT}}} \tag{Eq. 7}$$

To analyze the current relaxation kinetics of Cx26, a monoexponential fitting of current traces was applied as shown in Equation 8,

$$I(t) = I_0e^{\frac{-t}{\tau}} + I_{ss} \tag{Eq. 8}$$

where $I(t)$ is the current at time t; I_0 is the current at time 0; and I_{ss} is the stationary state current. The exponential factor τ is the time constant, which in a two-state system is determined by the inverse of the sum of the forward and reverse reaction rates α and β, respectively. This is shown in Equation 9.

$$\tau = \frac{1}{\alpha + \beta} \tag{Eq. 9}$$

In a voltage-dependent channel, α and β are voltage-dependent and can be expressed as shown in Equations 10 and 11,

$$\alpha(V) = \alpha_0e^{\frac{z\alpha FV}{RT}} \tag{Eq. 10}$$

$$\beta(V) = \beta_0e^{\frac{z\beta FV}{RT}} \tag{Eq. 11}$$

where α_0 and β_0 are the values of α and β at 0 mV, and $z\alpha$ and $z\beta$ are the equivalent charges of α and β. Because of the differences in the kinetics of slow and fast gating, the fast gate can be approximated as a quasi-two-state process, and the voltage dependence of the fast gate in Cx26 hemichannels can be obtained.

The logarithms of the time constant *versus* voltage data were fitted with a linear regression separately for the activation (α) or deactivation (β) of the fast gate. Voltage dependence of the rates was obtained from the slope of these fittings.

Fitting of the three-state model was done with the Solver complement of Excel (Microsoft). Fitting of the current traces was done using the Levenberg-Marquardt algorithm built in the pClamp software (Axon). The linear fitting and graph figures were done with Prism (GraphPad). The optimization of parameters was performed by minimizing squared errors.

Kinetic Modeling—Cx26 ionic currents were simulated with the IonChannelLab software (27) using our kinetic model. The rates and z values for the transition between O_1 and O_2 were taken from Table 2. Because we cannot directly determine

the rates and individual z values for the slow gate (transition between C and O_1), they were estimated from our data (Table 3), assuming $\tau = 22$ s for the slow gates at -50 mV and a z for the $O_1 \to C$ transition of 0.2 reported previously (28).

Molecular Modeling—As there is no experimental structure for rat Cx46 and mouse Cx50, comparative structural models were generated for this study, using the Modeler software (29) and taking the structure of human Cx26 (Protein Data Bank code 2ZW3) as a template. To start building the models, the alignments of each target sequence and the structural template from our alignment of non-redundant Cx sequences were extracted, and gap-only regions were eliminated. Ten models were generated in each case, and those with the lowest discrete optimized protein energy (DOPE) score (29) were selected as the final models.

Missing residues of human Cx26 were inserted with Modeler. This was performed by generating models of the human Cx26 structure, using the full sequence of human Cx26 as the target, and the structure of Cx26 (Protein Data Bank code 2ZW3) as a template. The backbone of the experimental Cx26 structure was fully conserved.

TABLE 3

Constrained parameters describing the voltage dependence of the slow gate of WT Cx26 and mutants

	WT Cx26	Cx26_K41N	Cx26_K41E_E42K
z_s (e_o)	2.01 ± 0.04	2.6 ± 0.2^a	2.1 ± 0.2
V_s (mV)	21 ± 1	-2 ± 3^b	-7 ± 2^b

^{a} $p < 0.05$ using two-tailed Student's t test. Data were calculated using Equation 6 constrained with the parameters obtained from kinetics.
^{b} $p < 0.01$ using two-tailed Student's t test. Data were calculated using Equation 6 constrained with the parameters obtained from kinetics.

Results

Cxs Do Not Show a Transmembrane Pattern of Charges Associated with Voltage Dependence—Non-redundant Cx sequences were aligned with MAFFT, as explained under "Experimental Procedures" (481 sequences were used). From this alignment, the sequences of several Cxs with known gap junctional voltage dependence were selected (12). This study specially focused on charges of the N terminus and TM-1 regions that were previously associated with voltage dependence and gating of Cxs (Fig. 1) (17, 22). Nevertheless, there is no clear pattern of charges that can explain the differences in voltage dependence among these Cxs, which is clearly evident when zebrafish Cx35 and mice Cx37 were analyzed, which, despite showing little difference in the distribution of charged residues, have a voltage dependence of about 1 elementary charge (e_o) and 11 e_o, respectively (30, 31). It is interesting to note that human Cx26 is the only Cx having a positively charged residue at the end of TM-1 (lysine 41). This lysine is conserved among different orthologs of Cx26 but is absent in all other Cx isoforms analyzed.

Determination of Voltage Dependence of Cx26 Hemichannels—To obtain the voltage dependence of the fast and slow gating mechanisms of Cx26, a tail current (I_{tail}) analysis was performed (Fig. 2A). Voltage pulse steps from -60 to $+60$ mV were applied to oocytes expressing Cx26 from a holding potential of $+30$ mV. The addition of 200 μM lanthanum (La^{3+}), which is a well known hemichannel inhibitor, completely eliminated these currents (Fig. 3A). Indeed, control oocytes injected only with the antisense oligonucleotide against the endogenous Cx38 showed currents similar to those recorded in the presence of La^{3+} (Fig. 3B). The $I(V)/I_{max}$ curve of the WT Cx26 showed a minimal conductance at voltages
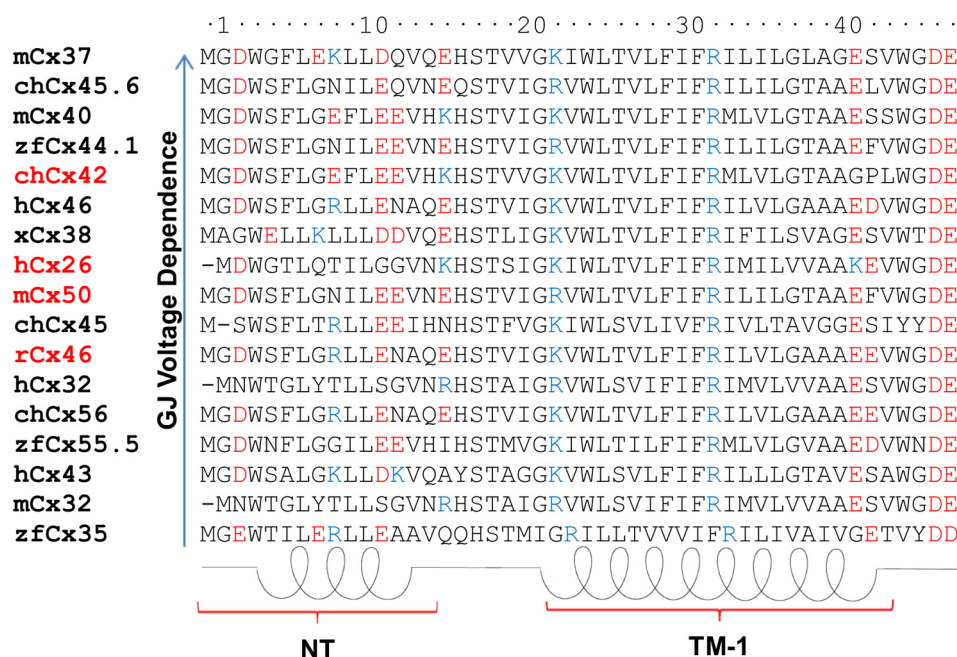

FIGURE 1. **Alignment of N terminus and TM-1 residues of connexin isoforms that exhibit different gap junctional voltage dependence.** Sequence alignments are displayed from connexins showing less (*zfCx35*, *bottom*) to more voltage dependence (*mCx37*, *top*). Basic and acidic residues are depicted in *blue* and *red*, respectively. Cx26, Cx42, Cx46, and Cx50 utilized in this work are in *red*. Amino acids residues are numbered according to the Cx26 sequence. *NT,* N terminus; *TM-1,* transmembrane domain-1; *ch,* chicken; *h,* human; *m,* mouse; *x, Xenopus*; *zf,* zebrafish. The values of voltage dependence were taken from Ref. 17.
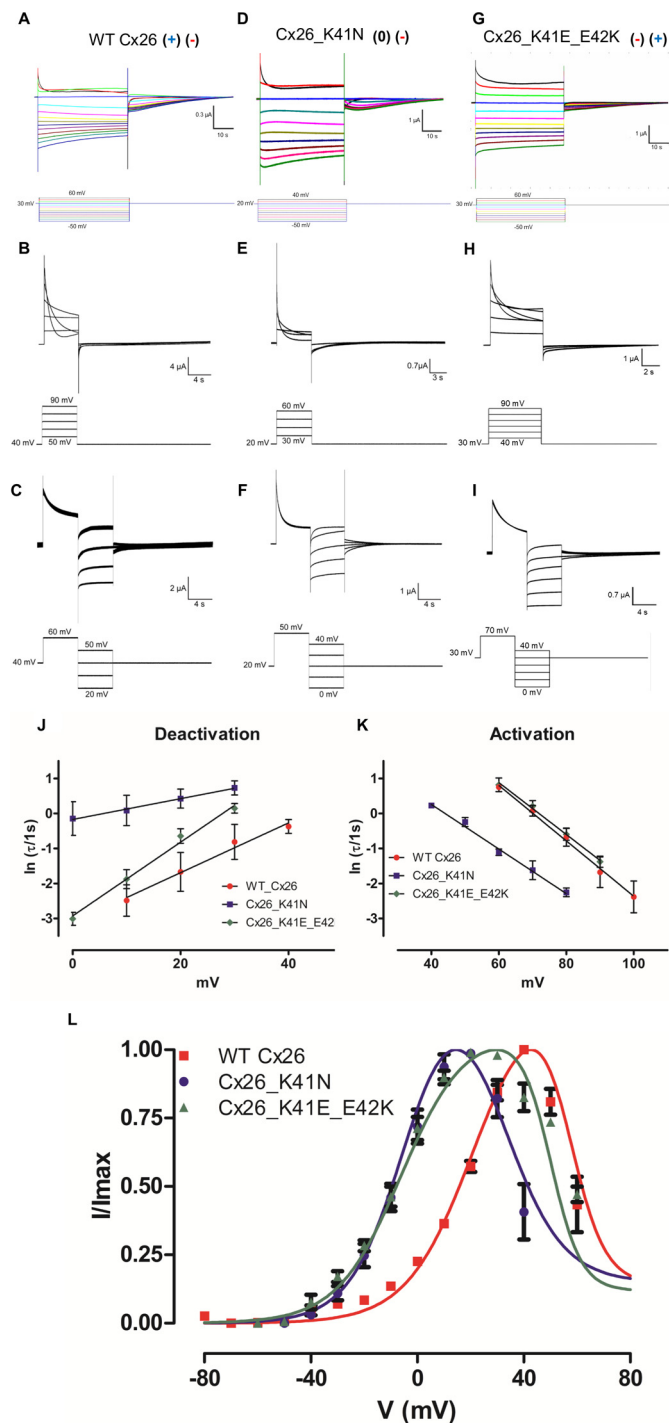
FIGURE 2. **Determination of voltage dependence in WT and mutant Cx26 hemichannels.** Oocytes bathed in extracellular solution and maintained in a holding potential of +30 mV (WT Cx26 and Cx26_K41E_E42K) or +20 mV (Cx26_K41N) were subjected to voltage pulses from −50 to +60 mV (WT Cx26 and Cx26_K41E_E42K) or + 40 mV (Cx26_K41N), and returned to holding potential. The currents are shown for oocytes expressing WT Cx26 (*A*), Cx26_K41N (*D*), and Cx26_K41E_E42K (*G*). The I/I_{max} relation of WT Cx26 (*red squares*), Cx26_K41N (*blue dots*), and Cx26_K41E_E42K (*green triangles*) mutants are shown (*L*). To determine the voltage dependence of activation and deactivation of the fast gate, differential voltage protocols were applied. Oocytes were bathed in extracellular solution and maintained at a holding potential of +40 (WT Cx26) + 30 (Cx26_K41E_E42K) or +20 (Cx26_K41N) mV. To obtain the activation reaction rates for WT Cx26 (*B*), Cx26 K41N (*E*), and Cx26_K41E_E42K (*H*) squared positive voltage pulses from +50 to +90 mV (WT Cx26), from +30 to + 60 mV (Cx26_K41N), or from +40 to +90 mV were used. To obtain deactivation reaction rates for the WT Cx26 (*C*), Cx26 K41N (*F*),
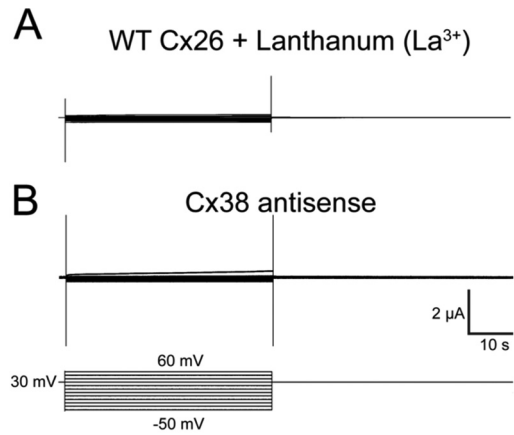

FIGURE 3. **Oocytes expressing human Cx26 in the presence of 200 μM La^{3+} (*A*) or injected with Cx38 antisense (*B*) do not show hemichannel currents.** Oocytes maintained in a holding potential of +30 were subjected to squared voltage pulses from −50 to +60 mV and returned to holding potential.

lower than −60 mV. Maximal tail current amplitude was at +40 mV and then started to decrease at more positive voltages (Fig. 2*L*, *red squares*). The slow gating process was defined by the ascendant part (or steepness) of the $I(V)/I_{max}$ curve. In contrast, fast gating promoted a decrease in the conductance at voltages larger than +40 mV. Endogenous currents developed at voltages higher than +60 mV, so the fast gating could not be evaluated at higher voltages using the $I(V)/I_{max}$ curve.
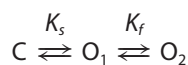
Because of difficulties in obtaining a reasonable amount of data points for the fast gate, the relaxation kinetics of the current at positive voltages was studied. To obtain the activation and deactivation rates of the fast gate, two different voltage protocols were used. First, the holding potential was set at +40 mV, where hemichannels exhibited maximal conductance. Squared pulses at higher voltages promoted an exponential current decay, which is related to the transition from the open to the subconductance state (Fig. 2*B*). A pulse to such higher potentials shifted the equilibrium to the subconductance state, which in turn decreased the current. To characterize the return from the subconductance to the open state, after the current decay was induced by a 60-mV pulse, decreasing voltage pulses within the range of 50 to 10 mV were applied to return to the open state (Fig. 2*C*). We avoided the activation of endogenous currents with the short test pulses used in these protocols (lasting only 5 s).

Because of the difference in kinetics of the slow gate and fast gate, with these voltage pulse protocols it was possible to

and Cx26_K41E_E42K (*I*) squared positive voltage pulses from +60 mV (WT Cx26), +50 mV (Cx26_K41N), or +70 mV (Cx26_K41E_E42K) were used to promote the population of the subconductance state, after which several negative voltage pulses were applied from +50 to +20 mV (WT Cx26) or from +40 to 0 mV (Cx26_K41N and Cx26_K41E_E42K). The current traces were fitted using an exponential decay function. The natural logarithm of τ versus voltage was plotted for the deactivation (*J*) and activation (*K*) of the fast gate. The voltage dependence of activation (α) and deactivation (β) was calculated from the slope of a linear regression of the data (straight lines, Equation 10 and 11), and the results can be seen in Table 2. To determine the voltage dependence of the slow gate, $I(V)/I_{max}$ curve was fitted using Equation 6 (*L*). The parameters utilized for the fast gate were taken from the kinetic analysis, and the results can be seen in Table 3. Current traces and corresponding voltage traces have the same color.

extract the kinetic parameters of the fast gate (see under "Experimental Procedures"). Fitting a mono-exponential decay (Equation 8) adequately described the current traces, whose time constant was used to determine the reaction rates of the fast gate. Voltage dependence was determined from a linear fit of the natural logarithm of the time constant *versus* the voltage curve for activation or deactivation (Equations 9–11) (Fig. 2, *J* and *K*, *red circles*). This method provided an accurate measurement of the voltage dependence of the fast gate, which was 3.9 e_0 (Table 2).

The establishment of a kinetic model was attempted to explain the transitions between the closed, the fully open, and the subconductance state of Cx26 hemichannels. Considering the existence of a closed (C), fully open (O_1) and subconductance (O_2) state, the three-state Model 1 was developed to describe Cx26 gating.

$$C \underset{}{\overset{K_s}{\rightleftharpoons}} O_1 \underset{}{\overset{K_f}{\rightleftharpoons}} O_2$$

Model 1

The only transitions allowed were $C \leftrightarrow O_1$ and $O_1 \leftrightarrow O_2$, and these were characterized by the K_s and K_f equilibrium constants representing the equilibrium constants of the slow and fast gates, respectively (see under "Experimental Procedures" for details). From the kinetic analysis of the fast gate, the z_f ($z_\alpha + z_\beta$) and V_f (the voltage at which $\alpha = \beta$) values were obtained (see Equations 2, 10, and 11) for the fast gate reducing to only two (z_s and V_s; see Equation 1) the number of parameters necessary to fit the whole $I(V)/I_{max}$ curve. By using this approach, it was possible to isolate the contribution of each gate in the $I(V)/I_{max}$ curve. This constrained the $I(V)/I_{max}$ curve (Fig. 2L, *red line*) gave a z_s of about 2.0 e_0 (Table 3).

The parameters determined from both the $I(V)/I_{max}$ curve fitting to the three-state model and the fast gate kinetic parameters were used to simulate the Cx26 hemichannel currents (see under "Experimental Procedures" for details). The simulations of Cx26 hemichannel currents under these conditions resembled the gating of the hemichannel (*cf.* Figs. 4B and 2A).

Mutation of Charged Residues at the End of TM-1 Modifies the Voltage Dependence of Cx26—Charged residues were replaced by polar amino acids using site-directed mutagenesis to investigate the role of the charged residues in the end of the TM-1 region. Among the neutralizations tested, only lysine 41 (Cx26_K41N) promoted changes in gating voltage dependence of the slow gate. Similar experiments as those described for the WT Cx26 were performed to determine voltage dependence of the Cx26_K41N mutant (Fig. 2, *D–F*). Voltage dependence for the fast gate was about 2.3 e_0. The difference with WT Cx26 was mainly due to the reduction of the deactivation voltage dependence in the mutant, as can be seen from the reduction in the slope of the deactivation graph of ln τ *versus* voltage (Fig. 2J, *blue squares*). V_f was shifted 20 mV to the left in the Cx26_K41N mutant (Fig. 2, *J* and *L*; Table 3). The Cx26_K41N mutant increased the voltage dependence of the slow gate to 2.6 e_0 compared with WT Cx26. Also, the V_s is leftward shifted from 21 to −2 mV (Fig. 3L, *blue circles*; Table 3).
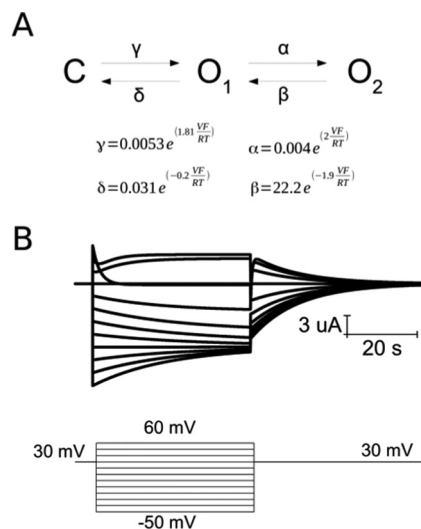

FIGURE 4. **Three-state model reproduces Cx26 hemichannel currents.** *A*, proposed kinetic model for Cx26 gating with the corresponding rate constants for the fast (α and β) and slow (γ and δ) gates and their voltage dependence. *B*, reproduction of current from Fig. 2A using the same voltage protocol over this kinetic model.

The increase in voltage dependence of the slow gate of the Cx26_K41N mutant suggests that lysine 41 acts as a countercharge in voltage gating, thereby decreasing voltage dependence. We tested whether other charges in this region could be playing the role of the "real" gating charge. Glutamate 42 was a candidate, but neutralization of glutamate 42 (Cx26_E42Q) or the double neutralization mutant Cx26_K41N_E42Q failed to show any hemichannel currents, and replacing lysine 41 with a glutamate residue (Cx26_K41E) did not show hemichannel currents either (Fig. 5, *A–C*).

When the charges of lysine 41 with glutamate 42 (Cx26_K41E_E42K) were swapped, hemichannel currents were observed (Fig. 2, *G–I*). In this case, the voltage dependence of the slow gate was unchanged and that of the fast gate was increased (Fig. 2L, *green triangles*; Table 3). The increase in the voltage dependence of the fast gate was due to an increase in the deactivation voltage dependence to about 2.6 e_0 (*cf.* Fig. 2, *J* and *K*, *green diamonds*; Table 2).

Comparative Analysis in Cx46—To analyze the involvement, the negatively charged residues present at the end of TM-1 on the voltage dependence of the slow gating of other Cxs, we focused in Cx46, which possesses two glutamate residues in this region. Glutamate 42 and glutamate 43 were neutralized, and their effects on the voltage dependence of the slow gate were analyzed. To our advantage, we found that in Cx46 there is no superposition in the activation of the slow and fast gate, and the I/I_{max} data for the slow gate can be fitted using a two-state Boltzmann equation (Equation 7). This fitting to the data (Fig. 6, *A–C* and *F*; Table 4) gave a $z\delta$ of about 2.8 e_0 for WT Cx46, 2.3 e_0 for the Cx46_E42Q mutant, and 2.4 e_0 for the Cx46_E43Q mutant. The Cx46_E42K mutant, which is reciprocal to the Cx26 sequence, decreased the voltage dependence of the slow gate to 2.2 e_0, and the Cx46_E43K mutant further decreased the voltage dependence to 1.8 e_0 (Fig. 6, *D–F*; Table 4). These results support our findings in Cx26, which suggested that neg-

A Cx26_E42Q (+) (0)

0.5 µA| 3 s

30 mV — 50 mV
-60 mV

B Cx26_K41N_E42Q (0) (0)

0.5 µA| 3 s

30 mV — 40 mV
-60 mV

C Cx26_K41E (+) (-)

0.5 µA| 3 s

30 mV — 50 mV
-60 mV

D Cx46_E42Q_E43Q (0) (0)
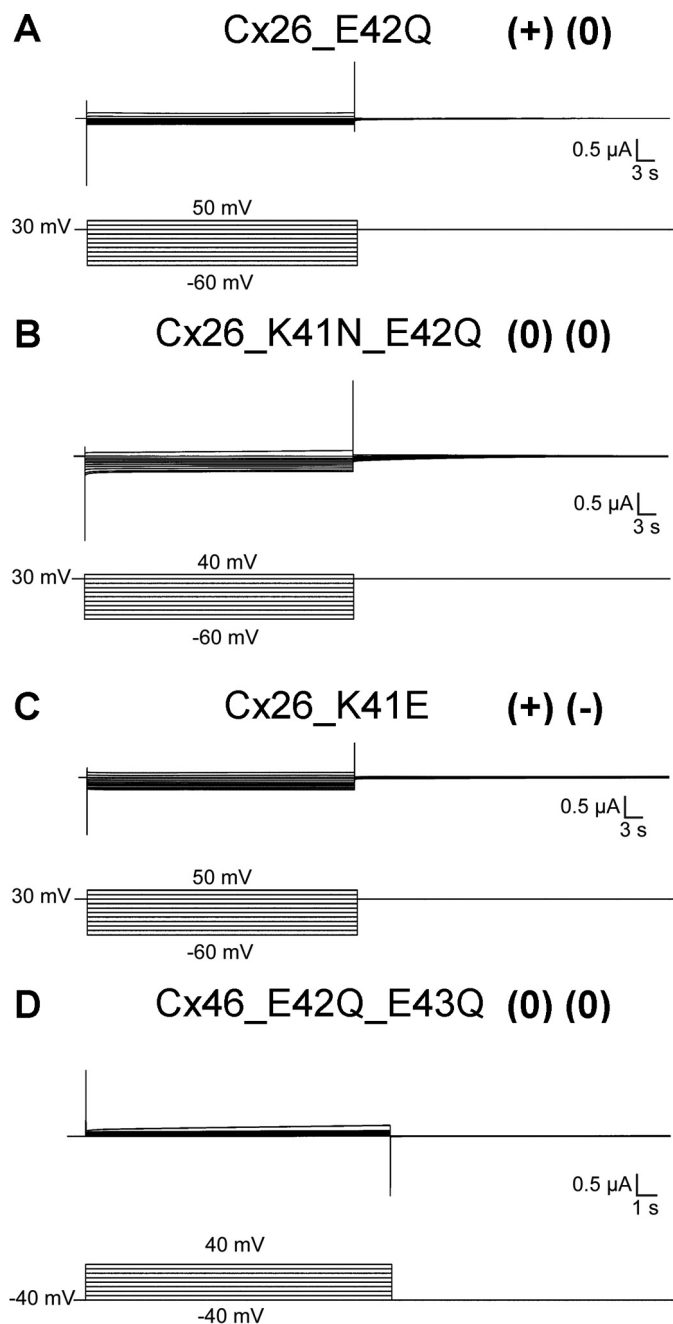
0.5 µA| 1 s

40 mV
-40 mV — -40 mV

FIGURE 5. **Mutation of charges at the end of TM-1 impairs hemichannel function.** Oocytes maintained at a holding potential of +30 (Cx26_E42Q, Cx26_K41N_E42Q and Cx26_K41E) or −40 mV (Cx46_E42Q_E43Q) were subjected to squared voltage pulses from −60 to 50 mV (Cx26_E42Q and Cx26_K41E), from −60 to 40 mV (Cx26_K41N_E42Q), or from −40 to 40 mV (Cx46_E42Q_E43Q) and returned to holding potential. Cx26_E42Q (*A*), Cx26_K41N_E42Q (*B*), Cx26_K41E (*C*), and Cx46_E42Q_E43Q (*D*) mutants do not show apparent hemichannel currents.

atively charged residues appreciably contribute to the total number of gating charges.

Comparative Analysis in Cx50—Most connexins in our alignment have only one negative charge in the region studied. We performed further experiments in one of these connexins, namely Cx50. The WT Cx50 possesses only one glutamate residue in position 42 and a phenylalanine residue in position 43, which are the correlative positions to those studied in Cx26 and Cx46 according to our alignment (Fig. 1). Glutamate 42 was

neutralized, and a phenylalanine 43 was replaced by a glutamate residue, and the effects of this on the slow gate voltage dependence were analyzed. The WT Cx50 channel has an apparent gating charge of 2.4 e_0 (Fig. 7, *A* and *D*; Table 5). The apparent gating charges decreased in the Cx50_F43E mutant to 2.0 e_0 and increased to 2.6 in the Cx50_E42Q mutant (Fig. 7, *B*–*D*; Table 5). This is clearly the inverse relation expected from our previous experience with Cx26 and Cx46.

Voltage Dependence of Cx42 Slow Gating—Cx42 does not have any charged residue in the studied region; it has glycine and proline residues instead. Still, this Cx formed functional GJC (45). Therefore, it was of interest to identify whether this Cx still displays voltage-dependent slow gating. The hemichannel currents of Cx42 display a voltage dependence of about 2.6 e_0 and V_s of −15 mV (Fig. 8; Table 6); these values are very similar to those obtained in the Cx50_E42Q mutant.

Position and Interaction of Residues at the End of TM-1—Our results in Cx26, Cx46, and Cx50 indicate that charged residues at the end of TM-1 contribute to the voltage dependence of these Cx hemichannels. According to the crystal structure of Cx26, lysine 41 interacts with glutamate 42 (Fig. 9, *A* and *D*). Nevertheless, most Cx isoforms have one or two negatively charged residues at the end of TM-1 (Fig. 1). In the homology model of Cx46, glutamate 42 takes the place of lysine 41 and interacts with glutamate 43, among other charged residues (Fig. 9, *B* and *E*). This is also found in the homology model of Cx50, where glutamate 42 takes the place of lysine 41, and phenylalanine 43 takes the position corresponding to glutamate 42 (Fig. 9, *C* and *F*). It is interesting to note that in the crystal structure and the homology models the arginine in position 75/76 and glutamate 46/47 interact with the residues studied. These interacting residues are highly conserved among the Cx family.

Discussion

Cxs are essential players in key physiological and pathological processes (32, 33). Thus, the study of the structural and functional properties of Cx-based channels is critical for understanding the physiological and pathological roles that Cxs may play. It is well known that Cxs are regulated by two voltage-gating mechanisms called fast and slow gating.

The fast gating mechanism has been proposed to arise from the pore region of the N terminus, which acts as a plug into the channel (3, 13). Alternative models for the fast gating mechanism is the ball-chain model, in which the interaction of the C terminus and the cytoplasmic loop region interact in a voltage- and pH-dependent manner, where this interaction would mediate the fast gating of the channel (34).

The mechanism underlying slow gating and the molecular determinants of its voltage dependence remain elusive. This study sought to address this issue and the role that charged residues at the end of the TM-1 region may play in this process. According to the Cx26 structure, in this region lysine 41 lines the pore and interacts with glutamate 42 (3). This region is proposed to undergo conformational changes during slow gating (15, 22, 35). Indeed, these residues have been previously reported to participate in the voltage dependence of GJs composed of Cx26 or Cx32 (10). However, the effects of these residues on the fast or slow gates, together with the amount of
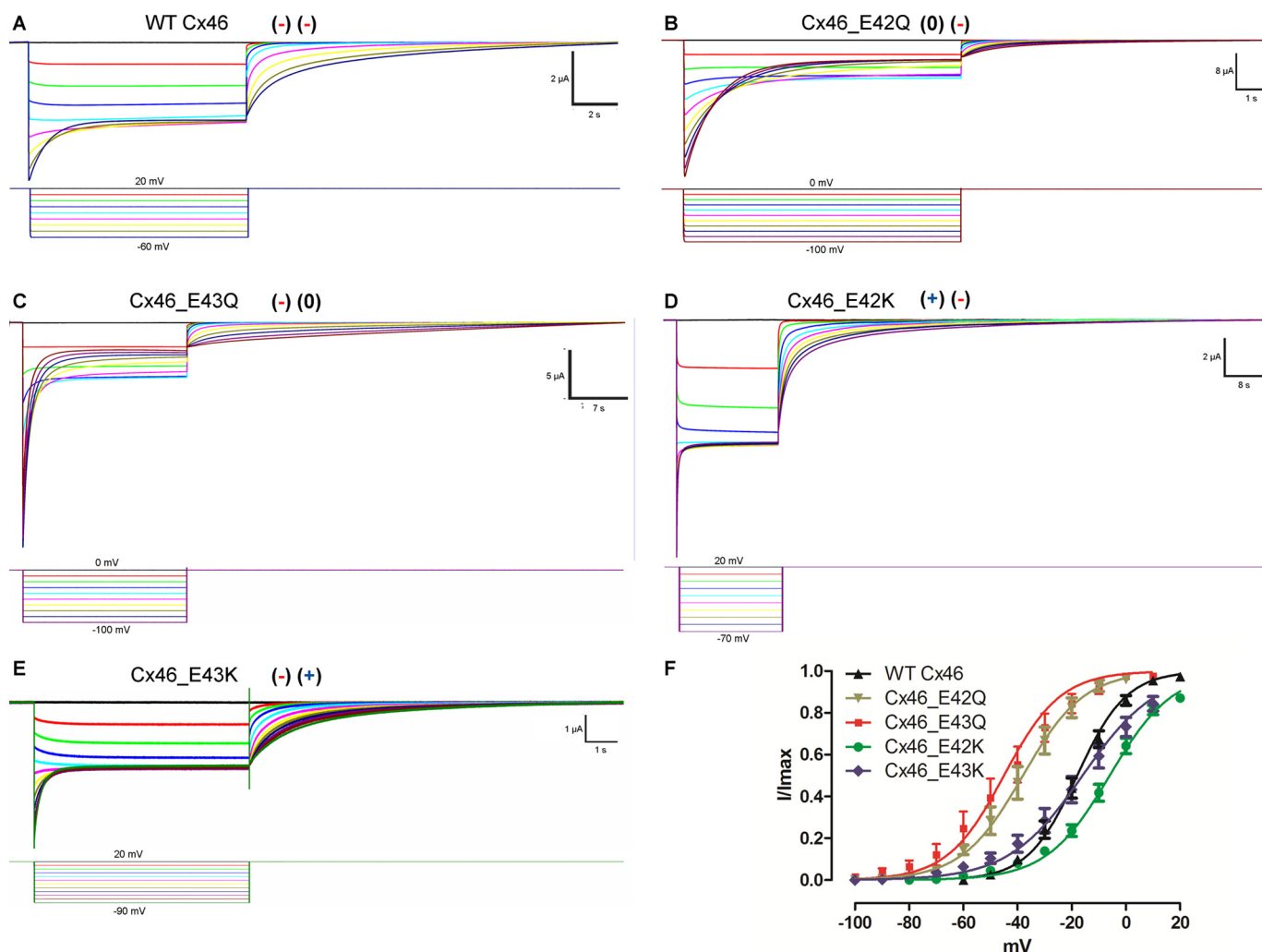
FIGURE 6. **Determination of voltage dependence of the slow gate in WT and mutant Cx46 hemichannels.** Oocytes maintained at a holding potential of +20 mV (WT Cx46, Cx46_E42K, and Cx46_E43K) or 0 mV (Cx46_E42Q and Cx46_E43Q) were subjected to hyperpolarizing pulses from 20 to −60 mV (WT Cx46), from 0 to −110 mV (Cx46_E42Q), from 0 to −100 mV (Cx46_E43Q), from 20 to −70 mV (Cx46_E42K), or from 20 to −90 mV (Cx46_E43K) and returned to holding potential. Hemichannel currents recorded in oocytes expressing Cx46 (*A*), Cx46_E42Q (*B*), Cx46_E43Q (*C*), Cx46_E42K (*D*), and (Cx46_E43K) (*E*) mutants. *F, graph* depicting the $I(V)/I_{max}$ relation of WT Cx46 (*black*), Cx46_E42Q (*brown*), Cx_E43Q (*red*), Cx_E42K (*green*), and Cx_E43K (*blue*) mutants. The *solid lines* represent the fitting of the data to Equation 7 and using the mean values in Table 4. Current traces and corresponding voltage traces have the same color.

TABLE 4
Parameters of the voltage dependence of the slow gate of WT Cx46 and mutants

	WT Cx46	Cx46_E42Q	Cx46_E43Q	Cx46_E42K	Cx46_E43K
z_s (e_o)	2.8 ± 0,1	2.27 ± 0.08[a]	2.4 ± 0.1[a]	2.20 ± 0.08[b]	1.8 ± 0.1[b]
V_s (mV)	−18 ± 2	−38 ± 3[b]	−45 ± 5[b]	−6 ± 2[b]	−15.96 ± 4

[a] $p < 0.05$ using two-tailed Student's *t* test. Data were calculated using Equation 7.
[b] $p < 0.001$ using two-tailed Student's *t* test. Data were calculated using Equation 7.

charge that each residue moves across the electric field, are still unknown.

It is clear from our sequence alignment that the voltage dependence of GJCs is neither explained by the amount nor the distribution of charged residues in the TM-1 or N terminus of the protein, although evidence mainly points to these regions as being responsible for voltage sensing in Cxs (10, 11, 17, 36). It is likely that voltage dependence in GJs depends on several factors, such as the contribution of both gating mechanisms, differences in the focusing of the electric field along the pore, or even the interaction between the two connexons. To obtain a clear picture of the role of the charged residues along the pore

in voltage dependence of Cx gating, the contributions of all these phenomena must be taken into account.

Using undocked hemichannels, in which both gating mechanism have differentiable contributions, is an efficient way to dissect the two gating mechanisms and hence analyze them separately. Here, Cxs whose hemichannels have a bell-shaped *G/V* curve were used. This made it possible to separate the fast and slow gating mechanisms. The steady state $I(V)/I_{max}$ relation and relaxation kinetics were analyzed to determine the voltage dependence of fast and slow gating of Cx26 hemichannels. The voltage dependence of Cx26 hemichannels can be well represented by a three-state linear model, considering the
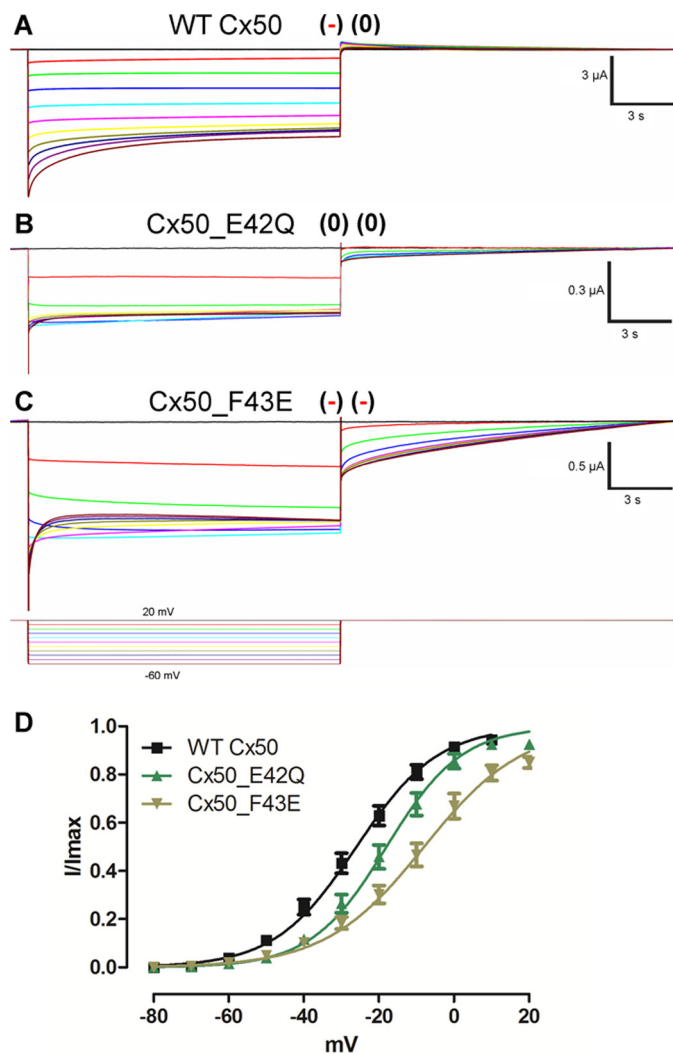
FIGURE 7. **Determination of voltage dependence of the slow gate in WT and mutant Cx50 hemichannels.** Square voltage pulses were applied to determine voltage dependence. Oocytes maintained in a holding potential of +20 mV were subjected to hyperpolarizing pulses from 20 to −60 mV. Hemichannel currents recorded in oocytes expressing Cx50 (*A*), Cx50_E42Q (*B*), and Cx50_F43E (*C*) mutants. *D*, graph depicting *I*(V)/*I*max relation of WT Cx50 (*black*), Cx50_E42Q (*green*), and Cx50_F43E (*brown*) mutants. The *solid lines* represent the fitting of the data to Equation 7 and using the mean values in Table 5. Current traces and corresponding voltage traces have the same color.

TABLE 5

Parameters of the voltage dependence of the slow gate of Cx50 and mutants

	WT Cx50	Cx50_E42Q	Cx50_F43E
z_s (e_0)	2.35 ± 0.06	2.56 ± 0.02^a	1.96 ± 0.06^b
V_s (mV)	-26 ± 2	-18.32 ± 2^a	-8.746 ± 3^b

[a] $p < 0.05$ using two-tailed Student's *t* test. Data were calculated using Equation 7.
[b] $p < 0.001$ using two-tailed Student's *t* test. Data were calculated using Equation 7.

closed (*C*), fully open (*O*$_1$), and subconductance (*O*$_2$) states. Simulating Cx26 hemichannel currents with this model and the experimentally determined parameters reproduces the currents observed in the voltage clamp experiments, thus further supporting our channel gating model.

Our results show that the neutralization of lysine 41 augments the equivalent charges of the slow gate but reduces those of the fast gate. Lysine 41 is conserved among different orthologs of Cx26, but not among Cx isoforms, because all other Cxs analyzed that were either negatively charged or neutral amino acids occupied this position. The effects of this neutralization on slow gating can be attributed to an unmasking of other charges that contribute to the gating. Based on its proximity and interaction with lysine 41, the best candidate for this putative gating charge is the adjacent negatively charged glutamate 42. When the charge swapping mutant Cx26_K41E_E42K was expressed in oocytes, the voltage dependence of the slow gate remained the same as the WT suggesting that the contribution of these charges to the voltage dependence is the same irrespective of their position. However, this mutant showed increased voltage dependence in the deactivation of the fast gate, and this suggest that the contribution of these charges to both gating processes might be through independent mechanisms. Unfortunately, the role of glutamate 42 and lysine 41 in Cx26 could not be studied in more detail because no currents were detected when Cx26_E42Q, Cx26_K41N_E42N, or Cx26_K41E mutants RNAs were injected in oocytes. It may be worth noting that the deletion of the Glu-42 residue is linked to genetic deafness and palmoplantar keratoderma (37).

To date, there is no direct evidence of coupling between the two gates. In fact, it has been recently described that the slow gate involves local rearrangements in the TM-1/EL-1, which by itself prevents the ion flux (15, 35). Considering the latter, the effect of lysine 41 neutralization and charge swapping challenges the idea that fast and slow gating act as separate mechanisms. Based on our results, it seems that modifications of one gate may affect the other and that the voltage sensor for both gates seems to be shared, at least in part.

Role of Negatively Charged Residues in the TM-1 of Cx46 and Cx50—The increase in the apparent gating charge of the Cx26_K41N mutant suggested that glutamate 42 may be a putative gating charge. Nevertheless, neutralization of this residue did not yield functional hemichannels. In the crystal structure of Cx26, it can be seen that lysine 41 is close enough to interact with glutamate 42. A screening effect of lysine 41 over glutamate 42 would explain the augmentation of gating charges due to the neutralization. To support the role of negative residues in this region, we generated the neutralization of the corresponding residues in rat Cx46. Cx46 has two glutamate residues in this region (glutamate 42 and glutamate 43), and the neutralization of each decreased the apparent gating charges of Cx46. The mutation of these glutamates to lysine augmented the difference, although slightly in the case of glutamate 42 and more heavily in glutamate 43. These results are consistent with those observed in Cx26. The differences in the actual values induced by neutralization or charge swap might be due to a change in profile of the electric field across the hemichannel pore.

Our results in Cx50 contradict our expectation. In this region, Cx50 has glutamate 42 and phenylalanine 43. When glutamate 42 was neutralized, the voltage dependence of the hemichannel increased, and when phenylalanine 43 was mutated by a glutamate, the voltage dependence decreased. This suggests that the movement of charges of Cx50 is reversed with respect to that of Cx26 and Cx46 hemichannels.
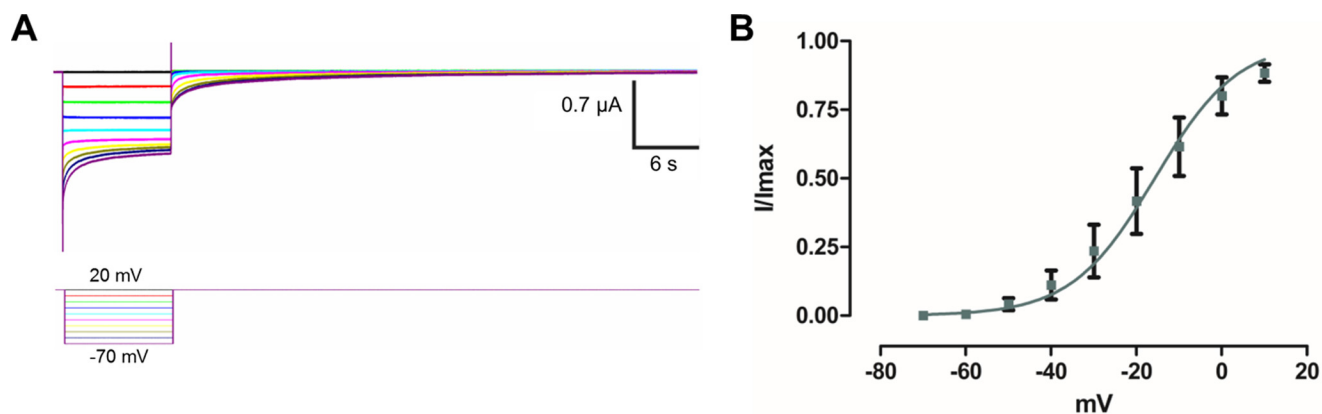
FIGURE 8. **Determination of voltage dependence of the slow gate in WT Cx42.** *A*, oocytes expressing Cx42 maintained at a holding potential of $+20$ mV were subjected to hyperpolarizing pulses from 20 to -70 mV and returned to holding potential. *B, graph* depicting the I(V)/I_{max} relation of Cx42. The *solid line* represents the fitting of the data to Equation 7 and using the mean values in Table 6. Current traces and corresponding voltage traces have the same color.

TABLE 6
Parameters of the voltage dependence of the slow gate of Cx42
Data were calculated using Equation 7.

	WT Cx42
$z_s\,(e_0)$	2.6 ± 0.2
$V_s\,(\mathrm{mV})$	-15 ± 5

It has been previously proposed that the addition of a glutamate residue in position 43 in chicken Cx45.6, which is an ortholog of human Cx50 (38), favored magnesium ion (Mg^{2+}) binding and thus promoted GJ closing (39). Additionally, replacing leucine 43 with glutamate in the Cx45.6–56M1 chimera (chicken Cx45.6 with the TM-1 of chicken Cx50) promoted an increase of 20% in the voltage dependence at negative potentials (39). These data indicate that adding negative charges in this region affects the voltage dependence of the slow gate in other Cx isoforms as well.

Several mutants in this region did not show hemichannel currents. It has been proposed that the surface electrostatic profile on the extracellular face of Cx50 is crucial for the trafficking of the hemichannel to the plasma membrane. It is likely that some of the mutations introduced affected the trafficking of the hemichannel, and consequently, we could not observe any hemichannel currents (40).

Voltage Gating in the Absence of Charges at the End of TM-1—One of the few Cxs that does not have any charges in the region studied is Cx42. It might be expected that the absence of charges and the presence of a proline residue might provide structural rigidity in this region, which could impair the slow gating mechanism. The *GV* curve of Cx42 is surprisingly similar to that of Cx50_E42Q mutant, in which charges are absent, too. This indicates that although the TM-1 charges studied here play a role in the slow gating mechanism, these are only part of the voltage-sensing machinery, and other charges or dipoles must be also involved in voltage sensing.

Proposed Mechanism of Slow Gating Based on the Action of Charged Residues in the TM-1 of Cx26, Cx46, and Cx50—The results obtained are consistent with the mechanism proposed for the loop gating mechanism in which a rotation and constriction of the TM-1 EL-1 region drives the closing of the GJ (15). This turn of the helix would move the charged residues away

from the pore of the channel to face the other transmembrane domains and expose nonpolar hydrophobic residues to the pore of the channel, such as valine and tryptophan. The exposure of these residues to the pore of the channel might generate a collapse of the pore due to hydrophobic interaction, creating a hydrophobic seal. This mechanism would explain the high degree coupling between the movement of the voltage sensor and the gating of the channel.

In the case of Cx50, contrary effects of charge substitutions suggest that the movement of this region during slow gating is inversed in relation to Cx26 and Cx46. In Cx50, it has been shown that mutation of phenylalanine 43 to cysteine locks the channel in a closed state, which is reversible upon the application of DTT or N,N,N′,N′-tetrakis(2-pyridylmethyl)ethylenediamine (TPEN) (22). This indicates that phenylalanine 43 residues are brought closer together during slow gating in the Cx50 hemichannel. This is contrary to the model for Cx32·43E1 (Cx32 with the EL-1 of Cx43), in which serine 42 (the equivalent position of phenylalanine 43) is moved further apart during slow gating and is not exposed in the closed conformation (15). The inverse movement of the TM-1 region might explain these conflicting results. It may also explain why adding a glutamate in Cx50 decreases voltage dependence, and the neutralization of glutamate 42 increases voltage dependence, which is clearly an effect contrary to that observed for Cx26 and Cx46. Further experimental information on the positioning of these residues in the open and closed conformation of these different Cxs would shed more light on the movement of the TM-1 during slow gate activation.

The crystal structure of Cx26 and the homology model of Cx46 and Cx50 show that two highly conserved residues within the Cx family (an arginine at position 75/76 and a glutamate in position 46/47) are interacting partners of glutamate 42/43. By using molecular simulation of the Cx26 hemichannel, it has been found that arginine 75 is part of an electrostatic network in which glutamate 42 and aspartate 46 also take part (41). Arginine 75 mutations in Cx26 cause genetic deafness (42), and several of these mutations generate aberrant gating of Cx26 hemichannels (43). Based on these results, it has been proposed that arginine 75 is part of the voltage sensor of Cxs. A possible role for arginine 75 is the stabilization of negative residues
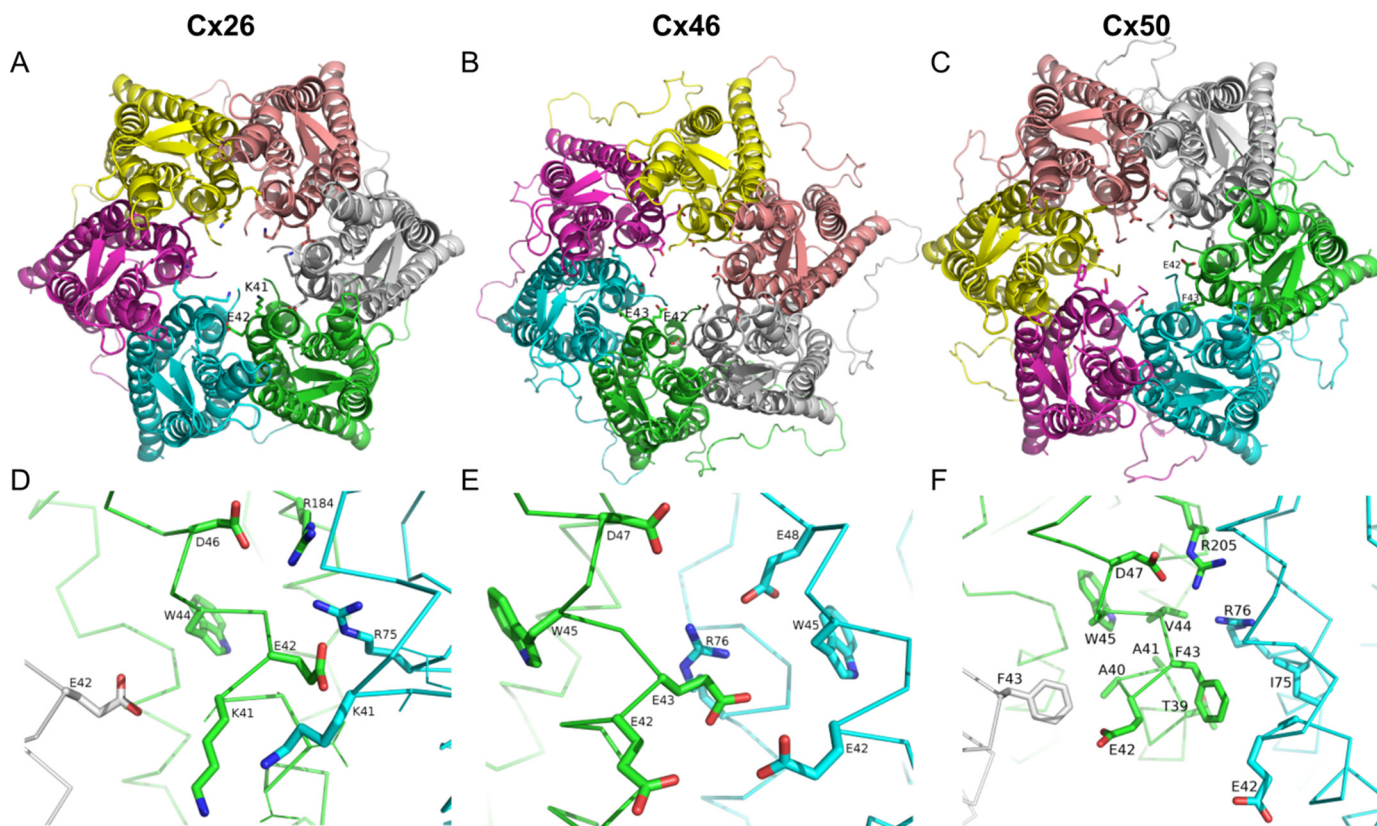
FIGURE 9. **Position and interaction of residues at the end of TM-1.** Extracellular view of human Cx26 (*A*), rat Cx46 (*B*), and mouse Cx50 (*C*) in schematic representation with side chains of residues Lys-41 and Glu-42 for Cx26 (*A*), residues Glu-42 and Glu-43 of Cx46 (*B*), and residues Glu-42 and Phe-43 of Cx50 (*C*) represented as *sticks*. Zooms in the lateral region around residues Lys-41 and Glu-42 in human Cx26 (*D*), Glu-42 and Glu-43 in rat Cx46 (*E*), and Glu-42 and Phe-43 in Cx50 (*F*). Side chain of these residues and possible interacting residues around 5 Å are represented as *sticks* and labeled. The panels were generated with PyMOL.

when they do not face the pore, similar to how acidic residues interact with arginines in the voltage sensor domain of the Shaker potassium channel (44) or the bacterial sodium channel (44).

On the Determination of Voltage Dependence in Cxs—It is of interest to note that the fast gate voltage dependence determined for Cx26 hemichannels is equal to the voltage dependence of GJCs (10). This suggests that the voltage dependence of Cx26, and possibly other GJ channels, may be mainly involved in the fast gate with little involvement in the slow gate.

Our results for the voltage dependence are in accordance with those published previously for Cx26 (21) and Cx46 (46). Nevertheless, they differ from previous literature in the case of Cx50 (20). This might be due to differences in length of the voltage pulse protocols. It was also noted that upon larger and extended hyper-polarizations, Cx50 hemichannel currents showed long lasting inactivation. A caveat in the determination of GJ and hemichannel voltage dependence is that it is usually determined by the "slope factor" A ($A = z\delta/RT$) of a Boltzmann equation (12, 21). The voltage dependence determined from the Boltzmann equation has been proven to be insufficient for other ion channels, such as the Hv1 proton channel (47) and the Shaker potassium channel (48). The adjustment to a simple two-state model of a more complex kinetic scheme might give an underestimation of the gating charges. Thus, the use of a two-state Boltzmann equation to fit the conductance-voltage data only provides a lower estimate of the gating charges. For

greater reliability, and to model independent values of the effective gating charges, the limiting slope analysis would be the best available methodology (49, 50). Future studies on the voltage dependence of Cxs should address this point.

Voltage Gating Process on the Pore—In this work we support the idea that Cxs sense the voltage drop across the pore of the channel through charges present in the N terminus and at the end of the TM-1 segment.

The mechanism of voltage gating in the pore is not unique to Cxs. The KcsA channel, which is a bacterial K^+ channel that contains only a pore domain composed of two transmembrane segments (51), shows a voltage-dependent gating of around 0.7 e_0 (52). This voltage dependence is eliminated when glutamate 71, which is a residue at the selectivity filter, is neutralized (52). Nevertheless, this glutamate does not seem to be exposed to the solvent, similar to residues that mediate voltage dependence in Cxs. However, several voltage sensor domains can act as ion-conducting pores. This is the case for proton currents generated when a basic residue in the S4 segment (Arg-371) of the *Shaker* K^+ channel is mutated to histidine (53) or in the voltage-gated Hv1 proton channel (54). In both cases, the activation of the voltage sensor and the opening of the ion-conducting pathway are merged. This might also be the case for Cx channels.

Conclusion—Our work has shown that residues at the end of the TM-1 contribute to the voltage dependence of the slow gating mechanism of Cx channels. However, the exact contribution in each Cx cannot be defined *a priori*. Other residues

involved in the voltage dependence of the slow gate have yet to be described.

References

1. Söhl, G., and Willecke, K. (2003) An update on connexin genes and their nomenclature in mouse and man. *Cell Commun. Adhes.* **10,** 173–180
2. Sosinsky, G. E., and Nicholson, B. J. (2005) Structural organization of gap junction channels. *Biochim. Biophys. Acta* **1711,** 99–125
3. Maeda, S., Nakagawa, S., Suga, M., Yamashita, E., Oshima, A., Fujiyoshi, Y., and Tsukihara, T. (2009) Structure of the connexin 26 gap junction channel at 3.5 A resolution. *Nature* **458,** 597–602
4. Harris, A. L. (2001) Emerging issues of connexin channels: biophysics fills the gap. *Q Rev. Biophys.* **34,** 325–472
5. Retamal, M. A. (2014) Connexin and pannexin hemichannels are regulated by redox potential. *Front. Physiol.* **5,** 80
6. Contreras, J. E., Sánchez, H. A., Eugenin, E. A., Speidel, D., Theis, M., Willecke, K., Bukauskas, F. F., Bennett, M. V., and Sáez, J. C. (2002) Metabolic inhibition induces opening of unapposed connexin 43 gap junction hemichannels and reduces gap junctional communication in cortical astrocytes in culture. *Proc. Natl. Acad. Sci. U.S.A.* **99,** 495–500
7. Lampe, P. D., and Lau, A. F. (2004) The effects of connexin phosphorylation on gap junctional communication. *Int. J. Biochem. Cell Biol.* **36,** 1171–1186
8. Contreras, J. E., Sáez, J. C., Bukauskas, F. F., and Bennett, M. V. (2003) Gating and regulation of connexin 43 (Cx43) hemichannels. *Proc. Natl. Acad. Sci. U.S.A.* **100,** 11388–11393
9. Palacios-Prado, N., and Bukauskas, F. F. (2009) Heterotypic gap junction channels as voltage-sensitive valves for intercellular signaling. *Proc. Natl. Acad. Sci. U.S.A.* **106,** 14855–14860
10. Verselis, V. K., Ginter, C. S., and Bargiello, T. A. (1994) Opposite voltage gating polarities of two closely related connexins. *Nature* **368,** 348–351
11. Harris, A. L., Spray, D. C., and Bennett, M. V. (1981) Kinetic properties of a voltage-dependent junctional conductance. *J. Gen. Physiol.* **77,** 95–117
12. González, D., Gómez-Hernández, J. M., and Barrio, L. C. (2007) Molecular basis of voltage dependence of connexin channels: an integrative appraisal. *Prog. Biophys. Mol. Biol.* **94,** 66–106
13. Oshima, A., Tani, K., Hiroaki, Y., Fujiyoshi, Y., and Sosinsky, G. E. (2007) Three-dimensional structure of a human connexin26 gap junction channel reveals a plug in the vestibule. *Proc. Natl. Acad. Sci. U.S.A.* **104,** 10034–10039
14. Trexler, E. B., Bennett, M. V., Bargiello, T. A., and Verselis, V. K. (1996) Voltage gating and permeation in a gap junction hemichannel. *Proc. Natl. Acad. Sci. U.S.A.* **93,** 5836–5841
15. Tang, Q., Dowd, T. L., Verselis, V. K., and Bargiello, T. A. (2009) Conformational changes in a pore-forming region underlie voltage-dependent "loop gating" of an unapposed connexin hemichannel. *J. Gen. Physiol.* **133,** 555–570
16. Barrio, L. C., Suchyna, T., Bargiello, T., Xu, L. X., Roginski, R. S., Bennett, M. V., and Nicholson, B. J. (1991) Gap junctions formed by connexins 26 and 32 alone and in combination are differently affected by applied voltage. *Proc. Natl. Acad. Sci. U.S.A.* **88,** 8410–8414
17. Purnick, P. E., Oh, S., Abrams, C. K., Verselis, V. K., and Bargiello, T. A. (2000) Reversal of the gating polarity of gap junctions by negative charge substitutions in the N terminus of connexin 32. *Biophys. J.* **79,** 2403–2415
18. Rubin, J. B., Verselis, V. K., Bennett, M. V., and Bargiello, T. A. (1992) Molecular analysis of voltage dependence of heterotypic gap junctions formed by connexins 26 and 32. *Biophys. J.* **62,** 183–193
19. Verselis, V. K., and Srinivas, M. (2008) Divalent cations regulate connexin hemichannels by modulating intrinsic voltage-dependent gating. *J. Gen. Physiol.* **132,** 315–327
20. Beahm, D. L., and Hall, J. E. (2002) Hemichannel and junctional properties of connexin 50. *Biophys. J.* **82,** 2016–2031
21. González, D., Gómez-Hernández, J. M., and Barrio, L. C. (2006) Species specificity of mammalian connexin-26 to form open voltage-gated hemichannels. *FASEB J.* **20,** 2329–2338
22. Verselis, V. K., Trelles, M. P., Rubinos, C., Bargiello, T. A., and Srinivas, M. (2009) Loop gating of connexin hemichannels involves movement of pore-lining residues in the first extracellular loop domain. *J. Biol. Chem.* **284,** 4484–4493
23. Boratyn, G. M., Schäffer, A. A., Agarwala, R., Altschul, S. F., Lipman, D. J., and Madden, T. L. (2012) Domain enhanced lookup time accelerated BLAST. *Biol. Direct* **7,** 12
24. Bairoch, A., and Apweiler, R. (1996) The SWISS-PROT protein sequence data bank and its new supplement TREMBL. *Nucleic Acids Res.* **24,** 21–25
25. Katoh, K., Misawa, K., Kuma, K., and Miyata, T. (2002) MAFFT: a novel method for rapid multiple sequence alignment based on fast Fourier transform. *Nucleic Acids Res.* **30,** 3059–3066
26. White, T. W., Bruzzone, R., Goodenough, D. A., and Paul, D. L. (1992) Mouse Cx50, a functional member of the connexin family of gap junction proteins, is the lens fiber protein MP70. *Mol. Biol. Cell* **3,** 711–720
27. Santiago-Castillo, J. A., Covarrubias, M., Sánchez-Rodríguez, J. E., Perez-Cornejo, P., and Arreola, J. (2010) Simulating complex ion channel kinetics with IonChannelLab. *Channels* **4,** 422–428
28. Lopez, W., Gonzalez, J., Liu, Y., Harris, A. L., and Contreras, J. E. (2013) Insights on the mechanisms of Ca^{2+} regulation of connexin26 hemichannels revealed by human pathogenic mutations (D50N/Y). *J. Gen. Physiol.* **142,** 23–35
29. Sali, A., and Blundell, T. L. (1993) Comparative protein modelling by satisfaction of spatial restraints. *J. Mol. Biol.* **234,** 779–815
30. McLachlan, E., White, T. W., Ugonabo, C., Olson, C., Nagy, J. I., and Valdimarsson, G. (2003) Zebrafish Cx35: cloning and characterization of a gap junction gene highly expressed in the retina. *J. Neurosci. Res.* **73,** 753–764
31. Willecke, K., Heynkes, R., Dahl, E., Stutenkemper, R., Hennemann, H., Jungbluth, S., Suchyna, T., and Nicholson, B. J. (1991) Mouse connexin37: cloning and functional expression of a gap junction gene highly expressed in lung. *J. Cell Biol.* **114,** 1049–1057
32. Saez, J. C., Berthoud, V. M., Branes, M. C., Martinez, A. D., and Beyer, E. C. (2003) Plasma membrane channels formed by connexins: their regulation and functions. *Physiol. Rev.* **83,** 1359–1400
33. García, I. E., Maripillán, J., Jara, O., Ceriani, R., Palacios-Muñoz, A., Ramachandran, J., Olivero, P., Perez-Acle, T., González, C., Sáez, J. C., Contreras, J. E., and Martínez, A. D. (2015) Keratitis-ichthyosis-deafness syndrome-associated cx26 mutants produce nonfunctional gap junctions but hyperactive hemichannels when co-expressed with wild type cx43. *J. Invest. Dermatol.* **135,** 1338–1347
34. Nielsen, M. S., Axelsen, L. N., Sorgen, P. L., Verma, V., Delmar, M., and Holstein-Rathlou, N. H. (2012) Gap junctions. *Compr. Physiol.* **2,** 1981–2035
35. Kwon, T., Tang, Q., and Bargiello, T. A. (2013) Voltage-dependent gating of the Cx32*43E1 hemichannel: conformational changes at the channel entrances. *J. Gen. Physiol.* **141,** 243–259
36. Kronengold, J., Srinivas, M., and Verselis, V. (2012) The N-terminal half of the connexin protein contains the core elements of the pore and voltage gates. *J. Membr. Biol.* **245,** 453–463
37. Rouan, F., White, T. W., Brown, N., Taylor, A. M., Lucke, T. W., Paul, D. L., Munro, C. S., Uitto, J., Hodgins, M. B., and Richard, G. (2001) trans-dominant inhibition of connexin-43 by mutant connexin-26: implications for dominant connexin disorders affecting epidermal differentiation. *J. Cell Sci.* **114,** 2105–2113
38. Jiang, J. X., White, T. W., Goodenough, D. A., and Paul, D. L. (1994) Molecular cloning and functional characterization of chick lens fiber connexin 45.6. *Mol. Biol. Cell* **5,** 363–373

39. Tong, J. J., and Ebihara, L. (2006) Structural determinants for the differences in voltage gating of chicken Cx56 and Cx45.6 gap-junctional hemichannels. *Biophys. J.* **91,** 2142–2154

40. Sarkar, D., Ray, K., and Sengupta, M. (2014) Structure-function correlation analysis of connexin50 missense mutations causing congenital cataract: electrostatic potential alteration could determine intracellular trafficking fate of mutants. *BioMed Res. Int.* **2014,** 673895

41. Kwon, T., Harris, A. L., Rossi, A., and Bargiello, T. A. (2011) Molecular dynamics simulations of the Cx26 hemichannel: evaluation of structural models with Brownian dynamics. *J. Gen. Physiol.* **138,** 475– 493

42. Richard, G., White, T. W., Smith, L. E., Bailey, R. A., Compton, J. G., Paul, D. L., and Bale, S. J. (1998) Functional defects of Cx26 resulting from a heterozygous missense mutation in a family with dominant deaf-mutism and palmoplantar keratoderma. *Hum. Genet.* **103,** 393–399

43. Deng, Y., Chen, Y., Reuss, L., and Altenberg, G. A. (2006) Mutations of connexin 26 at position 75 and dominant deafness: essential role of arginine for the generation of functional gap-junctional channels. *Hearing research* **220,** 87–94

44. Blanchet, J., Pilote, S., and Chahine, M. (2007) Acidic residues on the voltage-sensor domain determine the activation of the NaChBac sodium channel. *Biophys. J.* **92,** 3513–3523

45. Barrio, L. C., Jarillo, J. A., Beyer, E. C., and Saéz, J. C. (1995) in *Progress in Cell Research* (Kanno, Y., Kataoka, Y., Shiba, Y., Shibata, T., and Shimazu, T., eds) pp. 391–394, Elsevier, Amsterdam

46. Ebihara, L., and Steiner, E. (1993) Properties of a nonjunctional current expressed from a rat connexin46 cDNA in *Xenopus* oocytes. *J. Gen. Physiol.* **102,** 59 –74

47. Gonzalez, C., Rebolledo, S., Perez, M. E., and Larsson, H. P. (2013) Molecular mechanism of voltage sensing in voltage-gated proton channels. *J. Gen. Physiol.* **141,** 275–285

48. Zagotta, W. N., Hoshi, T., Dittman, J., and Aldrich, R. W. (1994) Shaker potassium channel gating. II: Transitions in the activation pathway. *J. Gen. Physiol.* **103,** 279 –319

49. Almers, W. (1978) Gating currents and charge movements in excitable membranes. *Rev. Physiol. Biochem. Pharmacol.* **82,** 96 –190

50. Bezanilla, F., and Stefani, E. (1994) Voltage-dependent gating of ionic channels. *Annu. Rev. Biophys. Biomol. Struct.* **23,** 819 – 846

51. Doyle, D. A., Morais Cabral, J., Pfuetzner, R. A., Kuo, A., Gulbis, J. M., Cohen, S. L., Chait, B. T., and MacKinnon, R. (1998) The structure of the potassium channel: molecular basis of K^+ conduction and selectivity. *Science* **280,** 69 –77

52. Cordero-Morales, J. F., Cuello, L. G., and Perozo, E. (2006) Voltage-dependent gating at the KcsA selectivity filter. *Nat. Struct. Mol. Biol.* **13,** 319 –322

53. Starace, D. M., and Bezanilla, F. (2001) Histidine scanning mutagenesis of basic residues of the S4 segment of the shaker K^+ channel. *J. Gen. Physiol.* **117,** 469 – 490

54. Tombola, F., Ulbrich, M. H., and Isacoff, E. Y. (2008) The voltage-gated proton channel Hv1 has two pores, each controlled by one voltage sensor. *Neuron* **58,** 546 –556